How enhancers regulate wavelike gene expression patterns: A novel enhancer prediction and live reporter system identifies an enhancer associated with the arrest of pair-rule waves in *Tribolium*

Christine Mau[1], Heike Rudolf[1], Frederic Strobl[2], Benjamin Schmid[3], Timo Regensburger[1], Ralf Palmisano[3], Ernst Stelzer[2], Leila Taher[4*], Ezzat El-Sherif[1*]

[1] Division of Developmental Biology, Department of Biology, Friedrich-Alexander-Universität Erlangen-Nürnberg, 91058 Erlangen, Germany.

[2] Buchmann Institute for Molecular Life Sciences (BMLS), Goethe-Universität Frankfurt Am Main, Frankfurt am Main, Germany.

[3] Optical Imaging Centre Erlangen (OICE), Friedrich-Alexander-Universität Erlangen-Nürnberg, 91058 Erlangen, Germany.

[4] Institute of Biomedical Informatics, Graz University of Technology, A-8010 Graz, Austria.

* Corresponding Authors: Ezzat El-Sherif (ezzat.elsherif@fau.de), Leila Taher (leila.taher@tugraz.at)

Abstract

A key problem in development is to understand how genes turn on or off at the right place and right time during embryogenesis. Such decisions are made by non-coding sequences called 'enhancers'. Much of our models of how enhancers work rely on the assumption that genes are activated de novo as stable domains of gene expressions that undergo little or no change, either indefinitely or until they do their job whereafter they gradually fade away. Such view has been strengthened by the intensive landmark studies of the early patterning of the anterior-posterior (AP) axis of the *Drosophila* embryo, where indeed gene expression domains seem to arise more or less simultaneously and stably. However, careful analysis of gene expressions in other model systems (including the AP patterning in vertebrates and short-germ insects like the beetle *Tribolium castaneum*) painted a different, very dynamic view of gene regulation with a strong temporal dimension, where genes are oftentimes expressed in a wavelike fashion. How such gene expression waves are mediated at the enhancer level is so far unclear. Here we establish the AP patterning of the short-germ beetle *Tribolium* as a model system to study dynamic and temporal pattern formation at the enhancer level. To that end, we established an enhancer prediction system in *Tribolium* based on time- and tissue-specific ATAC-seq and an enhancer live reporter system based on MS2 tagging. Using this experimental framework, we discovered several *Tribolium* enhancers, and assessed the spatiotemporal activities of some of them in live embryos. We found our data consistent with a model in which the timing of gene expression during embryonic pattern formation is mediated by a balancing act between enhancers that induce rapid changes in gene expressions (that we call 'dynamic enhancers') and enhancers that stabilizes gene expressions (that we call 'static enhancers').

Introduction

While an embryo is growing, each cell continuously receives inputs from surrounding cells. The cell processes these inputs and decides its fate accordingly. This decision-making process relies on non-coding sequences called 'enhancers' (1,2). Much of our models of how enhancers work during development relies on the assumption that genes are activated de novo across embryonic tissues as stable domains of gene expressions (3–5), that then undergo little or no change, either indefinitely or until they do their job whereafter they gradually fade away. Such a view has been strengthened by the intensive landmark studies of the early patterning of the anterior-posterior (AP) axis of the fruit fly *Drosophila melanogaster* embryo, where indeed gene expression domains seem to arise more or less stably (reviewed in (6–9)). However, careful analysis of gene expressions in other model systems painted a different, very dynamic view of gene regulation. For example, during the AP patterning of vertebrates, oscillatory waves of gene expressions were shown to sweep the embryo before they stabilize into their final positions (6,10,11), demarcating future vertebrae. Likewise, Hox genes propagate along the AP axis of vertebrates, demarcating future axial identities (6,12,13). In both neural tube and limb bud of vertebrates, gene expressions arise in a temporal sequence and spread across the tissue, dividing them into different embryonic fates (14–19).

Surprisingly, patterning of the AP axis of insects, the same process that popularized the static view of gene regulation, turned out to be much more dynamic than previously thought. In insects, the AP axis is divided into segments via the striped expression of a group of genes called 'pair-rule' genes, and into domains of different axial fates via the expression of a group of genes called 'gap genes' (6,7). In the flour beetle *Tribolium castaneum* (*Tribolium*), it has been shown that both pair-rule and gap genes are expressed as dynamic waves that propagate from posterior to anterior (20–24), much like how segmentation and Hox genes are expressed in vertebrates (6). Even pair-rule and gap genes in *Drosophila*, classically thought to be expressed stably, have recently been shown to undergo dynamic posterior-to-anterior shifts (25–29), a phenomenon that has been suggested to be an evolutionary vestige of outright gene expression waves (6,30–33).

These observations show that the static view of gene regulation, once popularized by classical studies of AP patterning in *Drosophila*, is the exception rather than the norm, and that gene regulation is in most cases a very dynamic phenomenon. Hence, new models of embryonic pattern formation need to be adopted, and concomitantly, new models of how enhancers work within these pattern formation models.

Some of the authors have recently suggested a model that explains the generation of either periodic or non-periodic waves of gene expressions, called the 'speed regulation' model (6,23,24,30,34). In this model, a morphogen gradient modulates the speed of either a molecular clock (to produce a periodic pattern) or a genetic cascade (to produce a non-periodic pattern). This scheme was shown to be able to produce (*in silico*) periodic waves in the former case, and non-periodic waves in the latter. Furthermore, a molecular model, called the 'Enhancer Switching' model has been suggested as a mechanism for how a morphogen gradient could fine-tune the speed of a clock or a genetic cascade, serving as a molecular realization of the speed regulation model (6,23,34). Much like a car is controlled by two pedals (gas and brake), the Enhancer Switching model posits that each gene within a genetic clock or a genetic cascade is regulated by two enhancers: one 'dynamic' that induces rapid changes in gene activity (equivalent to a car's gas pedal), and another 'static' that stabilizes it (equivalent to a car's brake pedal). By modulating the balance between the potency of dynamic vs static enhancers, the tuning of speed of gene regulation is achieved. The model is partially supported by observations in the *Drosophila* embryo, where the gap gene *Kruppel* (*Kr*) was shown to be regulated by two enhancers with the predicted dynamics of the Enhancer Switching model, and that both enhancers mediated the observed dynamic shifts of *Kr* along

the *Drosophila* AP axis (23,26). Similar observations were made for the *Drosophila* gap gene *giant* (*gt*) (35).

However, the observed gene expression dynamics of *Drosophila* gap genes are vestigial, not outright waves of the sort observed during the AP patterning of vertebrates or short-germ insects like *Tribolium*. Hence, we sought to test the predictions of our 'Enhancer Switching' model in a system where 'canonical' gene expression waves are observed. We thought that the AP patterning of *Tribolium* serves our purpose well, and more generally, is an excellent model system to study enhancer regulation of dynamic gene expressions in general. First, *Tribolium* exhibits robust systemic RNAi, which greatly eases the generation of RNAi knockdowns using parental RNAi (36–39). Second, AP patterning takes place in the early *Tribolium* embryo, which eases the interpretation of RNAi knockdowns generated using parental RNAi, without the need of generating time-specific or tissue-specific genetic perturbations. Indeed, most genetic interactions between gap and pair-rule genes in *Tribolium* have been elucidated by a handful of labs over a few years since the discovery of the efficacy of parental RNAi in *Tribolium* (23,24,40–50). Third, several genetic and genomic tools have been developed for *Tribolium* (51): transgenesis (52,53), transposon-based random mutagenesis (54), large-scale RNAi screens (39), CRISPR-Cas9 (55,56), live imaging (21,57–59), and a tissue culture assay (21,60). Fourth, the *Tribolium* genome is compact compared to vertebrate model systems, rendering enhancer discovery more tractable in *Tribolium*.

Hence, in this work we aimed to test how enhancers mediate the generation of gene expression waves in *Tribolium*. To that end, we (i) discovered enhancer regions that regulate early patterning genes in *Tribolium*, and (ii) characterized the spatiotemporal dynamics of these enhancers.

Several strategies can be used to predict enhancer regions, each with their own advantages and disadvantages. In the Assay for Transposase-Accessible Chromatin with high-throughput sequencing (ATAC-seq), sequencing adapters are inserted into open regions of the genome using hyperactive mutant Tn5 Transposase (61). ATAC-seq is a fast and sensitive method, and requires very little embryonic tissues (often one embryo, or even a tissue dissected from one embryo) compared to other open chromatin assays. Assaying open chromatin (especially using ATAC-seq) is a popular method for enhancer discovery as it does not require antibodies. However, not all open chromatin regions are active enhancers. Chromatin is also accessible at promoters, insulators, and regions bound by repressors (62–65), and hence, enhancer discovery using open chromatin assays has a high false positive rate. Interestingly, chromatin accessibility has been shown to be dynamic across space and time at active developmental enhancers compared to other regulatory elements like promoters (66–68), and hence, dynamic chromatin accessibility has been proposed as an accurate predictor for active enhancers.

The second step to understand how enhancers mediate gene expression waves is to characterize the spatiotemporal dynamics driven by the discovered enhancers. *In situ* staining of carefully staged embryos can go a long way in characterizing dynamic gene expressions. However, salient features of these dynamics can be missed using this strategy, and a strategy to visualize enhancer activities in live embryos is thus needed. Using fluorescent proteins (FP) as reporter genes of enhancer activities have been traditionally the method of choice in live imaging studies. However, FPs suffer from low degradation rates, which results in averaging out fast changing gene expressions, rendering them unsuitable for visualizing highly dynamic gene activities. This problem can be circumvented by using a destabilized version of FPs (69). However, the reported reduction in FP, although decent, is not enough to detect fast dynamics of many developmental genes. Moreover, destabilized FP suffers from low fluorescent intensity (70). Another strategy is to tag RNAs (71), like in MS2 tagging (72). In MS2 tagging, MS2 tandem repeats are inserted within a reporter gene. Upon reporter gene activation, the MS2 repeats are transcribed into stem loops that readily bind MS2 virus coat protein (MCP). If MCP-FP fusion proteins are ubiquitously present

in the background, they will then be recruited at the transcription site in as many numbers as transcribing RNA polymerases actively transcribing the reporter gene, offering a natural form of signal amplification. This strategy can be used to visualize de novo transcription (26,27,73–75) (in addition to estimate total mRNA counts, if a large number of MS2 repeats are used (76)), avoiding the averaging effect of using FPs as reporters.

In this work, we established a framework for enhancer discovery and enhancer activity visualization in live embryos in *Tribolium*. Previously, some of the authors participated in developing an enhancer discovery framework using whole embryo FAIRE-seq analysis in *Tribolium* (77). Here, we developed a modified enhancer discovery framework by assaying dynamic open chromatin in space and time in *Tribolium*, using tissue- and time-specific ATAC-seq. We then established an MS2-MCP system in *Tribolium* to visualize activity dynamics of the discovered enhancers, and developed computational methods to analyze the imaged activities in live embryos. Using both our enhancer discovery and visualization system, we show that some of the discovered enhancers regulating gap and pair-rule enhancers feature expression patterns that are in line with the 'Enhancer Switching' model.

Results

Profiling the chromatin accessibility landscape along the AP axis of the early *Tribolium* embryo

Genomic regions of increased chromatin accessibility are typically endowed with regulatory activity (68,78). To profile the accessible chromatin landscape of the developing *Tribolium* embryo, we performed ATAC-seq (61) on anterior (a), middle (m) and posterior (p) germband samples collected at two time points (IT23: 23-26 h after egg lay (AEL) and IT26: 26-29 h AEL; Materials and Methods). Our experimental design included six sample groups with 2-3 biological replicates. We generated and sequenced 17 ATAC-seq libraries to an average depth of 1,835,762 unique, high-quality pairs of reads (3.6X genomic coverage, Materials and Methods). Biological replicates of our ATAC-seq libraries were highly similar with a median Spearman's correlation coefficient of 0.875 (**Supplementary Figure 1**), demonstrating the reproducibility of the data. ATAC-seq has been successfully used to study the chromatin state of several organisms, including *Drosophila* (79), but we are not aware of previous applications of ATAC-seq to *Tribolium*.

We identified a total of 12,069 chromatin accessible sites (Materials and Methods), with 4,017 being specific to one or two particular regions of the germband and 1,610 to a given time point (**Supplementary Figure 2**). In agreement with the ability of ATAC-seq to detect distal regulatory elements in the genome (61), a large proportion of these sites were intergenic or intronic (46%, **Supplementary Figure 3**). Principal component analysis (PCA) of most variable accessible sites (Materials and Methods) mainly separated the samples along the AP axis of the embryo (**Figure 1A-C**), with the first principal component (PC1) accounting for 45.3% of the variance; PC2 (18.0% of the variance) predominantly distinguished the middle of the germband from its anterior and posterior ends. Among all 12,069 sites, 3,106 (26% of the accessible genome) were differentially accessible when compared between different regions along the AP axis and/or time point (Materials and Methods); for 1,049 of those sites, changes in accessibility were observed in four or more comparisons, indicating more intricate and, generally, specific patterns of accessibility (**Supplementary Figure 4**). Remarkably, while 62% of the constitutively accessible sites corresponded to promoters and gene bodies, 66% of the differentially accessible sites were intergenic or intronic, and this proportion was even higher (74%) among the differentially accessible sites with more specific patterns of accessibility (**Figure 1D**), suggesting that spatiotemporal control of transcription in the early *Tribolium* embryo is largely mediated by enhancers as opposed to promoters. Accessible sites were enriched for binding sites of several transcription factors (Materials and Methods; **Supplementary**

Figure 5). In particular, motifs consistent with the binding sites of 20 different transcription factors (Abd-A, Abd-B, Ap, Awh, Cad, CG18599, CG4328, E5, Ems, Eve, Ind, Lab, Lbe, Lbl, Lim3, Pb, PHDP, Pho, Vfl, and Zen) were enriched among all types of sites, independently of their accessibility dynamics.

When comparing accessibility along the AP axis at a particular time point, 2,109 sites were differentially accessible, the majority of them along the AP axis at 26 hours AEL. In addition, only 132 sites were differentially accessible between 26 and 23 hours AEL at the same portion of the embryo (**Supplementary Figure 4B and 4C**). To gain a better insight into the spatial and time dynamics of chromatin accessibility, we clustered all differentially accessible sites across the germband regions and time points (**Figure 1E**). Almost half of the sites were either not accessible in the anterior region of the embryo but accessible in the middle and posterior regions (cluster 4,756 sites), or not accessible in the middle and posterior regions of the embryo but accessible in the anterior region (cluster 5,698 sites). Approximately 25% of the sites showed predominantly monotonic changes in accessibility along the AP axis at 23 hours AEL, either increasing (clusters 3,420 sites) or decreasing (cluster 2,347 sites) from the anterior towards the posterior region of the embryo. Fifteen-percent of the sites showed similar accessibility levels in the anterior and middle part of the embryo, and decreased accessibility in the anterior part of the embryo (cluster 6,477 sites). Finally, 13% of the sites were most accessible in the middle region of the embryo (cluster 1,408 sites). The sites exhibited similar trends along the AP axis at both time points, although with the exception of the sites in clusters 2 and 4, the sites were generally more accessible at 26 hours AEL than at 23. Functional enrichment analysis of the gene nearest to each site (Materials and Methods) revealed that while all clusters are associated with “developmental process” and “anatomical structure development”, clusters 1 and 3 are specifically related to “pattern specification process” and “regionalization” and cluster 3 is specifically associated with “anterior/posterior pattern specification” (**Supplementary Figure 6**).

Together, our findings indicate that changes in chromatin accessibility in *Tribolium* at this developmental stage are primarily associated with space rather than time, and are particularly evident when comparing the anterior part of the germband to the middle and posterior parts.

Assaying chromatin accessibility is a popular method for enhancer discovery (68,78). However, not all open chromatin regions are active enhancers. To test for enhancer activity, we established an MS2-MCP enhancer reporter system in *Tribolium*.

Establishing an MS2-MCP enhancer reporter system to visualize enhancer activity in fixed and live *Tribolium* embryos

The established MS2-MCP enhancer reporter system is capable of visualizing enhancer activity in both fixed and live *Tribolium* embryos. To that end, we created two piggyBac reporter constructs (**Figure 2A and 2B**): an enhancer>MS2-*yellow* construct and an aTub>MCP-mEmerald construct. For the enhancer>MS2-*yellow* line, we placed the sequence of the putative enhancer which activity to be assessed upstream of the *Drosophila* Synthetic Core Promoter (DSCP) and a reporter gene composed of 24 tandem repeats of the MS2 stem loop inserted in the 5′ UTR of the *yellow* reporter gene (MS2-*yellow*), followed by an SV40 poly(A) tail. For the aTub>MCP-mEmerald line, we created a piggyBac construct in which the ubiquitous alpha-tubulin promoter was placed upstream of a nuclear localization sequence and the MCP-mEmerald fusion, followed by an SV40 poly(A) tail.

To visualize enhancer activity in fixed embryos, *in situ* staining for the *yellow* gene was applied to embryos carrying the enhancer>MS2-*yellow* construct. For visualization of enhancer activity in live embryos, a male beetle carrying the enhancer>MS2-*yellow* construct is crossed with a female beetle carrying the aTub>MCP-mEmerald construct. If active, the enhancer should drive the expression of the MS2-*yellow*

reporter in the progeny. The transcribed MS2 loops would then recruit aTub>MCP-mEmerald fusion proteins at the transcription site of the reporter gene, enriching the mEmerald fluorescent signal against the weak mEmerald background (**Figure 3A and 3B**). In this way, the intensity of de novo transcription driven by the enhancer can be assessed.

Via piggyBac transgenesis, we successfully generated a transgenic beetle line carrying the MCP-mEmerald construct, in which a ubiquitous mEmerald fluorescence is detected. We then sought to test our enhancer>MS2-*yellow* reporter system, using a previously discovered enhancer (hbA) that drives the anterior expression of the *Tribolium* gap gene *hunchback* (*hb*). Via piggyBac transgenesis, we successfully generated a transgenic beetle line carrying the hbA>MS2-*yellow* construct. Examining *yellow* expression using *in situ* hybridization chain reaction (HCR) staining in early hbA>MS2-*yellow* embryos (**Figure 2C**), we confirmed that the *yellow* expression in hbA>MS2-*yellow* line is similar to the mCherry expression in a previously tested hbA>mCherry line.

To test the live imaging capability of our MS2-MCP system, we crossed the hbA>MS2-*yellow* line with the aTub>MCP-mEmerald line. We could detected enriched puncta of mEmerald fluorescence in the early *Tribolium* embryo, whose spatial distribution across the embryo resembles that indicated by *in situ* staining of the *yellow* reporter gene (**Figure 3B and 3C**). This confirms that we succeeded in establishing an MS2-MCP enhancer reporter system that is capable of visualizing enhancer activity in both fixed and live *Tribolium* embryos.

Testing putative enhancers suggested by our ATAC-seq analysis

We then sought to use our enhancer reporter system to test putative enhancers suggested by our ATAC-seq analysis. In selecting a set of putative enhancers to test, we restricted out analysis to genomic regions around three genes involved in AP patterning in *Tribolium*: the gap genes *hb* (**Figure 4A**) and *Kr* (**Supplementary Figure 7G**) as well as the pair-rule gene *runt (run*) (**Figure 4B**). Enhancer regions were chosen based on ATAC peaks showing non-differential or differential accessibility and tested for enhancer activity.

Out of 9 tested reporters, 4 successfully drove *yellow* expressions in the early *Tribolium* embryo. The gap gene *hb* is expressed in multiple domains and regions in the early *Tribolium* embryo: in the serosa, in an anterior domain, in a secondary posterior domain, and in the nervous system (**Figure 4C**). The expression driven by hbB only overlaps with *hb* expression in the serosa, while hbA overlaps with the anterior expression of *hb*. Enhancer runA drove an expression in the nervous system that partially overlaps the endogenous *run* expression in the nervous system during the late germband stage. runB drove a striped expression in the ectoderm, partially overlapping endogenous *run* expression in the ectoderm, but not the striped *run* expression in the mesoderm, and the nervous system expression.

Testing the Enhancer Switching model

Next, we thought to test a molecular model for how to generate gene expression waves during development, suggested by some of the authors, namely: the Enhancer Switching model. The model predicts that for a gene involved in generating gene expression waves, there exists two enhancers: one dynamic enhancer responsible for initiating the wave, and another static enhancer responsible for arresting the wave into a stable gene expression domain (**Figure 5A-C**).

Among the discovered enhancers in *Tribolium*, two enhancers are potentially involved in generating gene expression waves: hbA and runB. The expression driven by both enhancers overlap with the gene expression waves of their corresponding genes: enhancer runB with the periodic waves of the pair-rule

gene *run*, and enhancer hbA with the non-periodic waves of the gap gene *hb*. To test if the spatiotemporal dynamics of these enhancers conforms with some of the predictions of the Enhancer Switching model, we first ran simulations of our Enhancer Switching model and carefully analyzed its predictions for the spatiotemporal dynamics of dynamic and static enhancers. Then, we used our enhancer reporter system to track the enhancer activity dynamics of runB and hbA in space and time using *in situ* HCR staining in carefully staged fixed embryos and live imaging.

Careful examination of the predictions of the Enhancer Switching model

Here we seek to carefully analyze the predictions of the Enhancer Switching model in space and time. To that end, we ran a simulation of a 3-genes realization of the periodic version of the model (**Figure 5B**, oscillator as dynamic module; Materials and Methods). Carefully analyzing model outputs for total activity of constituent genes, static enhancer reporters, and dynamic enhancer reporters revealed three characteristics of the spatiotemporal dynamics of their activities (**Figure 5C**). First, the activities of constituent genes, their dynamic enhancers, and static enhancers, are all expressed in waves that propagate from posterior to anterior. Second, the expression driven by dynamic enhancers progressively decreases in the posterior-to-anterior direction, while the expression driven by static enhancers progressively increases in the posterior-to-anterior direction. This is a natural consequence of the activating vs repressing effect of the speed regulator (which is expressed in a posterior-to-anterior gradient) on dynamic vs static enhancers, consequently. Third, the temporal activities of the dynamic enhancers are in phase of the total expressions of the genes they regulate and delayed from static enhancer activities.

Testing if runB matches the predictions of the Enhancer Switching model using in situ HCR staining

To test these predictions, we examined the spatiotemporal dynamics of one of the primary pair-rule genes, *run*, simultaneously with those of one of its enhancers, runB, using HCR in carefully staged embryos (**Figure 6A**). At the onset of segmentation (14 hours AEL), endogenous *run* expression forms a small cap at the posterior end of the blastoderm that progressively propagates towards anterior, whereas runB>*yellow* expression is still invisible. At 17 hours AEL, *run* expression clears from posterior forming a stripe at the posterior. Only then, runB>*yellow* expression arises, forming an overlapping stripe with *run* stripe at the anterior. At 20 hours AEL, the second wave of *run* arises at the posterior, while runB>*yellow* forms only a single stripe overlapping with the now stabilized first stripe. Only at 23 hours AEL, the second stripe of runB>*yellow* expression arises, overlapping with the new stabilized second *run* stripe. This overall behavior then cyclically repeats: stripes of runB>*yellow* expression arise only anteriorly, overlapping the stabilized *run* stripes. Of note, unlike the total expression of *run*, runB driven *yellow* expression progressively increases in the posterior-to-anterior direction. This is in line with predicted enhancer dynamics of our model, in which runB acts as a static enhancer of the gene *run*. First, runB drives gene expression waves that propagate from posterior to anterior. Second, the expression driven by static enhancers progressively increases in the posterior-to-anterior direction, reflecting the progressive drop of the speed regulator (suggested in *Tribolium* to be encoded directly or indirectly by Caudal; **Figure 6B**). Third, runB expression is delayed compared to *run*.

Testing if runB matches the predictions of the Enhancer Switching model using live imaging

To verify that runB drives expression in waves that propagate from posterior to anterior, we performed a live imaging analysis of runB driven expression using the MS2-MCP system. Crossing runB enhancer reporter line (driving an MS2-*yellow* reporter) with our aTub>MCP-mEmerlad line, and imaging early embryo of the progeny, we observed weak and diffuse mEmerald signal within the nuclei. In addition, we observed bright puncta within nuclei at a rate of at most one puncta per nucleus. The bright mEmerald puncta are distributed along the AP axis as a stripe resembling the *yellow* expression of the runB enhancer reporter visualized using *in situ* HCR staining (**Figure 6C and 6D**). We conclude, therefore, that such bright mEmerald puncta are mEmerald enrichment at transcribed MS2 loops, reflecting de novo transcription driven by the runB enhancer (henceforth called 'MS2 signal'). Hence, both individual nuclei of the early *Tribolium* embryo and de novo transcription driven by the runB enhancer can be visualized and detected in a single cross of runB>MS2-*yellow* line and the MCP-mEmerald line. To characterize the spatiotemporal activity of runB enhancer, circumventing the ambiguity introduced by nuclear flow, we developed programs to track the nuclei of the early live *Tribolium* embryo, detect MS2 puncta, and associate detected MS2 puncta to corresponding nuclei. To estimate accumulated mRNA signal (reflected by MS2 signal) based on de novo transcription, we computationally applied a moving average window to MS2 signal across time. Tracking the estimated mRNA signals in space, after discounting nuclear flow, revealed that runB indeed drives a wave of activity that propagates from posterior to anterior (**Figure 6B**, Right: Kymograph), verifying one of the predictions of our Enhancer Switching model.

Testing if hbA matches the predictions of the Enhancer Switching model using in situ HCR staining

As mentioned above, gap genes are expressed as well in waves in the *Tribolium* embryo, albeit in a non-periodic fashion in contrast to pair-rule waves. Gap gene waves are initialized by a pulse of *hb* expression that arises in the posterior of the blastoderm at 14 hours AEL, then eventually propagates towards anterior, clears from posterior, forming a stripe of *hb* expression at the anterior part of the embryo. Similar to our study of *run* vs runB driven *yellow* expression, we performed an analysis of the spatiotemporal dynamics of *hb* versus one of its enhancers hbA. We found that in the initiation phase of *hb* expression, hbA>*yellow* is still silent. Only when *hb* expression forms a stripe at the anterior, hbA>*yellow* expression arise forming an overlapping stripe with *hb* (**Figure 3C**). These dynamics are similar to those of a dynamic enhancer. However, simulations of varying static enhancer strength (**Supplementary Figure 8**) could lead to the impression of dynamic enhancer activity although the enhancer drives the whole expression pattern.

Assessing the correlation between differential accessibility and enhancer activity

We assessed the correlation between differential peak accessibility and enhancer activity using our tested enhancer constructs and previously published *Tribolium* enhancers of *single-minded* (*sim*) and *short gastrulation* (*sog*) (80) as well as of *labial* (*lab*), *Dichaete* (*D*) and *wingless* (*wg*) (81) (**Supplementary Figure 8**).

In total, eleven enhancer constructs were analyzed, where 54.5 % of constructs (six constructs) were active and 45.5 % of constructs were not active (five constructs). Five out of six active constructs are associated with sites that are differentially accessible, while one active construct overlaps with a site that is not differentially accessible. Two out of five not active constructs match sites that are not differentially accessible, while the remaining three not active constructs are associated with sites that are differentially accessible (**Figure 4D**; see **Supplementary Figure 7** for details). Therefore, about 60 % of analyzed differentially accessible peaks were associated with working enhancer constructs whereas in about 40 % of analyzed cases differentially accessible peaks could be found at non-working enhancer regions. In contrast, about 70 % of analyzed non-differentially accessible peaks were associated with non-working enhancer constructs. About 30 % of analyzed non-differentially accessible peaks are associated with working enhancer regions (**Figure 4E**). Thus, differential peak accessibility seems to be positively correlated with enhancer activity.

Discussion

In this paper, we established a framework for enhancer discovery in *Tribolium* using tissue- and time-specific ATAC-seq. We showed that differential peak analysis of tissue- and time-specific ATAC-seq yields a sizeable increase in enhancer prediction accuracy in *Tribolium*. We also developed an MS2 tagging and live imaging analysis framework in *Tribolium*. Both enhancer discovery and activity visualization systems are efforts to establish the AP patterning in *Tribolium* as a model system for studying dynamic gene expressions, especially gene expression waves, in development. Our experimental frameworks are suitable to explore how enhancers mediate dynamic gene expression in an unbiased fashion. However, in this work we set to test a specific model: the 'Enhancer Switching' model, a scheme some of the authors have recently suggested (23,34) to elucidate how gene expression waves, a phenomenon commonly observed during embryonic development (6,82,83), are generated at the molecular level. The model predicts that each patterning gene is simultaneously wired into two gene networks: (i) a dynamic network that drives sequential or periodic gene activities, and (ii) a static network that stabilizes gene activities into gene expression domains. The genetic wiring of each gene is encoded by two enhancers: (i) a dynamic enhancer that encodes the wiring of the gene within the dynamic gene networks, and (ii) a static enhancer that encodes the wiring of the gene within the static gene network. In this paper, we characterized computationally how the model predicts the spatiotemporal activities of enhancer reporters of dynamic and static enhancers. We found that the model predicts that reporter constructs of static enhancers should drive very distinctive spatiotemporal dynamics that coincides only with the late stabilization phase of the total gene expression patterns of genes, whereas dynamic enhancers drive expression patterns more or less similar to the expression patterns of the genes they regulate. We then used our enhancer discovery framework to discover a number of enhancers regulating embryonic patterning in the early *Tribolium* embryo. One of these enhancers, runB, drove an expression pattern consistent with a role as a static enhancer for the pair-rule gene *run*. Another enhancer, hbA drove expression patterns that is consistent with a role as a dynamic enhancer for the gap gene *hb*. However, the expression pattern driven by hbA could be also interpreted as driving the entirety of *hb* expression. We present these findings as tentative support for the 'Enhancer Switching', whereas a strong support requires: (1) finding (at least one) enhancer pair(s) whose activity dynamics match the predictions for static and dynamic enhancer for several gap and pair-rule genes, and (2) deleting either the dynamic of static enhancers result in the

predicted phenotypes. Future works should aim at testing these predictions, modifying the model, or finding alternative models. The methodologies for enhancer discovery and activity visualization established in this paper are steps towards this goal.

Materials and Methods

Beetle Cultures

Beetle cultures were reared on flour supplemented with 5 % dried yeast in a temperature- and humidity-controlled room at 24 °C. To speed up development, beetles were reared at 32 °C.

PiggyBac Enhancer Reporter Constructs

A piggyBac plasmid with the 3 x P3-mCherry/mOrange marker construct and multiple cloning sites (53) was used to make all enhancer constructs in this study. For enhancer constructs, putative enhancer regions, the *Drosophila* synthetic core promoter (77,84), and the MS2-*yellow* reporter gene (73,75) were amplified by PCR, assembled through ligation, and inserted into the multiple cloning site of the piggyBac plasmid. Used primers are listed in **Supplementary Table 1**.

Creation of the MCP-mEmerald construct

An artificial sequence, consisting of (i) an AscI restriction enzyme site, (ii) the *Tribolium* castaneum Georgia2 (GA2) background strain-derived (85) tubulin alpha 1-like protein (aTub) promoter (86), (iii) a *Tribolium* castaneum codon-optimized open-reading frame consisting of (a) the SV40-derived nuclear localization signal (NLS) tag (87) coding sequence, (b) the human influenza hemagglutinin (HA) tag (88) coding sequence and (c) the bacteriophage MS2 coat protein (MCP) (89) coding sequence, and (iv) a NotI restriction enzyme site, was de novo synthesized and inserted into the PacI/SacI restriction enzyme site pair of pMK-T (Thermo Fisher Scientific) by the manufacturer. The resulting vector was termed pGS[aTub'NLS-HA-MCP]. The sequence was excised with AscI/NotI and inserted into the backbone of the accordingly digested pACOS{#P'#O(LA)-mEmerald} vector (53). The resulting vector was termed pAGOC{aTub'NLS-HA-MCP-mEmerald}, contained (i) an expression cassette for mEmerald-labeled (90) and NLS/HA-tagged MCP, (ii) the piggyBac 3' and 5' inverted terminal repeats (91), as well as (iii) mOrange-based (92) and mCherry-based (93) eye-specific (94) transformation markers, and was co-injected with the standard piggyBac helper plasmid (95) into *Tribolium* castaneum embryos following standard protocols (96,97) to achieve germline transformation.

Tribolium Transgenesis

PiggyBac constructs were transformed into vermilion^{white} (98) with mCherry/mOrange as visible makers. Germline transformation was carried out using the piggyBac transposon system (95,99).

Egg Collections for Developmental Time Windows

Developmental time windows of three hours were generated by incubating three hours egg collections at 24 °C for the desired length of time. Beetles were reared in flour supplemented with 5% dried yeast.

In Situ Hybridization and Imaging of Fixed Embryos

In situ hybridization was performed using the third generation *in situ* hybridization chain reaction method (100). All probe sets and hairpins were ordered at Molecular Instruments. Lot numbers of probe sets are as follows: PRA978 (*run* mRNA), PRA979 (*hb* mRNA), and PRC655 (*yellow* mRNA). Images were taken with a Leica SP5 II confocal. A magnification of 20x was used at a resolution of 2,048 x 1,024. Images were processed and enhanced for brightness and contrast using Fiji (101).

Live Imaging

ATub>MCP-mEmerlad females were crossed with hbA>MS2-*yellow* or runB>MS2-*yellow*males. Three hours egg collections were generated and incubated for eleven (crossing with hbA) or fourteen hours (crossing with runB) at 24 °C. Embryos were dechorionated by immersion in 1 % bleach for 30 s twice. Embryos were mounted using the hanging drop method, with halocarbon oil 700 (Sigma). Time-lapse movies were taken by capturing 41 planes every 3 min, over ~ 6 h at 21 °C with a Leica SP5 II confocal. A magnification of 63X was used at a resolution of 1,024 x 900.

ATAC-seq library preparation

Embryos of the nGFP line (21) were collected in flour (+ 5 % yeast) for 3h and incubated for desired time length at 24 °C. Embryos were dechorionated by immersion in 1 % bleach for 30 s twice. Selected embryos were dissected into three parts (anterior, middle, and posterior). For each biological replicate, three of the same embryo parts were pooled, and three replicates were prepared for each sample condition. Library preparation was performed as previously described (79,102). Tagmentation was performed for 8 min. ATAC-seq libraries were sequenced on an Illumina NovaSeq 6000 at the Novogene Cambridge Genomic Sequencing Centre. 2x150 bp paired-end Illumina reads were obtained for all sequenced ATAC-seq libraries.

ATAC-seq data pre-processing

Sequencing reads were trimmed with cutadapt with parameters "-u 15 -U 15 -q 30 -m 35 --max-n 0 -e 0.10 -a CTGTCTCTTATA -A CTGTCTCTTATA" to remove adapter sequences and mapped to the *Tribolium castaneum* reference genome (Tcas5.2, GCA_000002335.3) with BWA-MEM (version 0.7.12-r1039). Next, read duplicates were marked with Picard MarkDuplicates (version 2.15.0). Low quality and duplicated reads were filtered using samtools view (version 1.10, (103)) with parameters "-F 1804 -f 2 -q 30". To flag regions that appear to be artifacts, we generated a blacklist using a strategy similar to the one developed by the ENCODE Project (104). Specifically, the genome was first divided into non-overlapping 50bp bins. Next, the BAM files containing the filtered mapped reads were converted into BigWig files using BAMscale (version 1.0, (105)) with parameters "scale --operation unscaled --binsize 20 --frag". Using the resulting BigWig files, the mean signal for each bin was computed across all sequencing libraries. Finally, bins with a mean signal equal to or greater than 100 were flagged as artifacts and included in a "blacklist". The threshold was determined by visual inspection of the distribution of the mean signals. Reads mapping to genomic regions in the blacklist were filtered out using samtools view (version 1.7, (103)) with parameters "-L" and "-U".

Peaks were called on individual replicates using macs3 (v3.0.0a7, https://github.com/taoliu/MACS; (106)) callpeak with parameters "-g 152413475 -q 0.01 -f BAMPE". The sets of peaks called in each sample were

then compared to each other and merged if they overlapped by at least 1 bp. Only merged peaks supported by peaks called in at least two different samples and on scaffolds assigned to linkage groups were considered for subsequent analyses. These peaks are further referred to as the set of “all” (consensus) chromatin accessible sites.

Chromatin accessible sites were annotated with HOMER (version 4.11.1, (107)) using the annotatePeaks.pl function.

Differential accessibility analysis

Differential accessibility analysis of the sites between different regions of the germband and/or time points was performed using the edgeR (version 3.36.0, (108)) and DESeq2 (version 1.34.0, (109)) methods within the DiffBind (version 3.4.11) R/Bioconductor package. Peaks with a false discovery rate (FDR) less than or equal to 0.05 for edgeR and/or DESeq were considered significant. Read counts for each peak were quantified with the dba.count() function, with parameters "score=DBA_SCORE_TMM_MINUS_FULL, fragmentSize=171, bRemoveDuplicates=TRUE". Briefly, this normalizes the read counts using Trimmed Mean of M-values (TMM, (110)) scaled by the full library size. We further refer to these values as “accessibility scores”. Sites that had a mean accessibility score larger than the median and a standard deviation larger than the 3rd quartile were defined as the “most variable accessible sites”.

Clustering

The z-score normalized accessibility scores of the differentially accessible sites were clustered using k-means (with k=6) as implemented in the kmeans() R function. The function was executed with default parameters except for “nstart=1000”, which initializes the algorithm with 1000 different sets of random centers and settles for those giving the best fit.

Complete linkage on the pairwise Pearson correlation distances (1-Pearson correlation coefficient) was performed with the hclust() R function to hierarchically cluster the differentially accessible sites based on their average accessibility scores across the replicates of each sample group. The pheatmap (version 1.0.12) R package was used for visualization using row-scaling.

Functional analysis

Functional enrichment analysis was carried out with the PANTHER API. Specifically, the “statistical enrichment test” tool was used with the “GO Biological Process complete” *Tribolium castaneum* database. Overrepresented GO terms/pathways were determined using default parameters (Fisher’s exact test, False Discovery Rate (FDR) < 0.05). All the positive overrepresented GO biological process (BP) terms were considered. The API was last accessed on August 2022.

Motif analysis

Motif enrichment analysis was carried out using XSTREME with default parameters except for “--streme-totallength 4000000 --meme-searchsize 100000 --ctrim 500 --streme-nmotifs 5” (version 5.4.0). Motifs discovered *de novo* were compared to the motifs in the insects JASPAR 2022 CORE non-redundant database (111) to identify putative transcriptional regulators. Sequences in which soft-masked nucleotides comprised 95% or more were not considered for the analysis.

Figure legends

Figure 1. Chromatin accessibility changes during AP axis patterning in the *Tribolium* embryo. (**A**) Principal component analysis (PCA) on the accessibility scores of the most highly accessible and variable sites in the dataset. PC analysis was performed using the PCA() function in the "FactoMineR" R package with default parameters. Only the first two principal components (PC) of the data are represented. The first PC explains 45.3% of the variance in the data, the second PC, 18.0%. (**B**, **C**) Boxplots showing the scores of PC1 and PC2 by space (B) and time (C). The thick line indicates the median (2nd quartile), while the box represents interquartile range (IQR, 1st to 3rd quartiles). Outliers are shown as dots. (**D**) Genomic annotation of different classes of chromatin accessible sites: all (consensus) sites, constitutive sites (i.e., consensus sites that are not differentially accessible), all differentially accessible sites, and most specifically accessible sites (i.e., sites differentially accessible in four or more comparisons). (**E**) K-means clustering of accessibility scores for differentially accessible sites. Accessibility scores have been z-score scaled for each site.

Figure 2. Analysis of hbA enhancer reporter construct. (**A**) Enhancer reporter construct. The DSCP drives expression of the *yellow* gene coupled to 24xMS2 stem loop sequences under the control of any enhancer of interest. (**B**) MCP-mEmerald construct. The ubiquitous aTub promoter drives expression of an MCP-mEmerald fusion gene containing a 5´ nuclear localization sequence. (**C**) Shown are the spatiotemporal dynamics of endogenous *hb* (green) and reporter gene *yellow* (red) expression in hbA embryos. Left: Shown are embryos from 14-26 h AEL at 24 °C. mRNA transcripts were visualized using *in situ* HCR staining on whole embryos. Nuclear staining in gray. Reporter gene *yellow* expression overlaps with endogenous *hb* expression at the posterior (merged in *yellow*). Posterior to the right. Right: Fluorescence signal along the dorsal-ventral axis was summed up to generate intensity distribution plots along the AP axis.

Figure 3. Analysis of hbA enhancer activity dynamics using the MS2-MCP live imaging system. (**A**) Overview image of an aTub>MCP-mEmerald embryo. (**B**) Embryo derived from an hbA>MS2-*yellow* x aTub>MCP-mEmerald crossing. Shown is a high resolution image of a blastoderm embryo exhibiting MS2-MCP signal (green dots). For computational image processing, nuclei showing green dots were tracked (white circle). (**C**) Computational image processing for live imaging movie. Left: Representative images over time. Nuclei were labeled in red if MS2-MCP signal (green) was detectable. Nuclei were kept for five time frames red with weakened red intensity. Middle: Intensity distribution plots along space for representative images. Right: Representation of the spatiotemporal hbA enhancer activity in a kymograph for all time frames of the live imaging movie.

Figure 4. Correlation of enhancer activity with differential accessibility. (**A, B**) ATAC profile for *hb* (A) and *run* (B). Enhancer regions at these loci are shown as boxes underneath the ATAC profiles. Differential ATAC peaks match well with active enhancer regions (purple boxes; red box: not active enhancer construct). (**C**) mRNA transcripts were visualized using *in situ* HCR staining on whole embryos (green: endogenous gene expression, red: reporter gene expression, *yellow*: merge). Nuclear staining in gray. hbA drives reporter gene expression in a stripe (embryo in germband stage shown). hbB drives reporter gene expression in the serosa (embryo in blastoderm stage shown). runA drives reporter gene expression in a subset of the endogenous *run* CNS expression (embryo in late germband stage shown). runB drives reporter gene expression in stripes, but is absent in the most posterior of the embryo. Posterior to the right. (**D**) Correlation between differential accessibility and construct activity. Differential peak analysis of ATAC peak sites. Eleven enhancer constructs were analyzed where 54.5 % of constructs (six constructs) were active and 45.5 % of constructs were not active (five constructs). Five out of six active constructs are associated with sites that are differentially accessible, while one active construct overlaps with a site that is not differentially accessible. Two out of five not active constructs match sites that are not differentially

accessible, while the remaining three not active constructs are associated with sites that are differentially accessible (see Supplementary Figure 7 for details). (**E**) Prediction efficiency based on differential peak analysis. Same enhancer constructs were analyzed as in (D). About 60 % of analyzed differential peaks were associated with working enhancers whereas in about 40 % of analyzed cases differential peaks could be found at non-working enhancer regions. In contrast, about 70 % of analyzed non-differential peaks were associated with non-working enhancer regions. About 30 % of analyzed non-differential peaks are associated with working enhancer regions.

Figure 5. Simulation of spatiotemporal dynamics of dynamic and static enhancer activity. (**A**) Cells can transit from one fate to another (fates depicted as blue, red, green, gold, and brown). The speed of this fate transition is dependent on the concentration of the speed regulator (gray). In the Speed Regulation Model, the speed regulator is applied as a gradient to pattern non-elongating tissues (e.g., the blastoderm). (**B**) A molecular realization of the Speed Regulation model is the Gradual Module Switching model composed of a dynamic and a static module. The dynamic module is a gene cascade (shown network, aperiodic gene activation, e.g., in the gap gene network) or an oscillator (shown network without solid *yellow* line, periodic gene activation, e.g., in the pair-rule gene network) activated by the speed regulator. The static module is a mutual exclusion gene network repressed by the speed regulator. Shown are three-gene regulatory networks (GRN) for the dynamic and static module (solid line: strong repression; dashed line: weak repression). A speed regulator gradient leads to a gradual switch from dynamic to static module activity. (**C**) Separate dynamic and static enhancers encode for the wiring of each gene in the GRNs. Enhancers for the red gene are shown. (**D**) Simulation of dynamic and static enhancer activity and resulting endogenous gene expression. Analyzed was their spatiotemporal behavior. Left: Intensity plots. Right: Kymographs. Figure panels A-C are adapted from (Zhu et al., 2017).

Figure 6. Analysis of runB enhancer activity dynamics using the MS2-MCP live imaging system. (**A**) Shown are spatiotemporal dynamics of endogenous *run* (green) and reporter gene *y* (red) expression in runB embryos. Left: Shown are embryos from 14-26 h AEL at 24 °C. mRNA transcripts were visualized using *in situ* HCR staining on whole embryos. Nuclear staining in gray. Reporter gene *y* expression partially overlaps with endogenous *run* expression (merged in *yellow*). Posterior to the right. Right: Intensity distribution plots along the AP axis. (**B**) Left: *In situ* HCR staining for endogenous *run* (green) and reporter gene y expression (red) combined with antibody staining for Cad protein (purple) on runB blastoderm (upper row) and germband embryos (lower row). Nuclear staining in gray. Posterior to the right. Right: Intensity distribution plots along the AP axis for the *yellow* region in the germband embryo. Cad formed a posterior-to-anterior gradient. runB drove strong y reporter gene expression outside of high Cad region (speed regulator in *Tribolium*). (**C**) Embryo derived from a runB>MS2-*yellow* x aTub>MCP-mEmerald crossing. Shown is a high resolution image of a blastoderm embryo exhibiting MS2-MCP signal (green dots). For computational image processing, nuclei showing green dots were tracked (white circle). (**D**) Computational image processing for live imaging movie. Left: Representative images over time. Nuclei were labeled in red if MS2-MCP signal (green) was detectable. Nuclei were kept for five time frames red with weakened red intensity. Middle: Intensity distribution plots along space for representative images. Right: Representation of the spatiotemporal runB enhancer activity in a kymograph for all time frames of the live imaging movie.

Supplementary Figure 1. Correlation between ATAC-seq sequencing libraries. Mapped sequencing reads of each biological replicate were used to calculate correlation between pairs of replicates. The values represent the Pearson correlation coefficients between pairs of sequencing libraries.

Supplementary Figure 2. Upset plot comparing the number of sites identified in samples corresponding to IT23 and IT26 as well as along the AP axis. (**A**) Plot corresponding to IT23 and IT26. (**B**) Plot corresponding to samples along the AP axis (a,m, and p). The number of sites in each of the sets considered is represented by the width of the bars in the bar chart at the bottom left. Each bar in the bar chart at the top represents the number of sites in an intersection. The intersection is indicated by filled circles below each bar. Note that the intersection sets are disjoint.

Supplementary Figure 3. Annotation of consensus sites. A total of 12069 ATAC peaks were analyzed. 22.3 %, 8.5 %, 23.5 %, 30.2 %, 15.5 % of these peaks overlap promoter-TSS, TSS, exon, intron, intergenic regions, respectively. TSS: Transcription Start Site.

Supplementary Figure 4. Differentially accessible sites. (**A**) The accessibility of the sites was compared between three different parts of the germband (anterior, middle, and posterior) at two time points (IT23 and IT26). All possible 15 comparisons were considered. A total of 3106 sites were differential accessible. (**B**) For the same part of the embryo, 132 sites were differentially accessible between two time points. (**C**) A total of 2109 sites were differentially accessible between two different parts of the germband at a given time point.

Supplementary Figure 5. Motif Analysis. Enrichment of TF motifs in accessible sites, depending on their accessibility (y-axis, see Figure 1D for details). The size of the dots represent the fraction of the sequences with one or more motif occurrences. The TFs (if known) are indicated on the x-axis.

Supplementary Figure 6. Functional enrichment analysis of the clusters of differentially accessible sites. Clustering of all differentially accessible sites across the AP axis and time points. All clusters are associated with "developmental process" and "anatomical structure development", while clusters 1 and 3 are specifically related to "pattern specification process" and "regionalization" and cluster 3 is specifically associated with "anterior/posterior pattern specification".

Supplementary Figure 7. Genomic tracks of previously analyzed enhancer reporter constructs. Genomic tracks of analyzed enhancer reporter constructs. (**A**) *labial* (*lab*) (**B**) *wingless* (*wg*) (**C**) *Dichaete* (*D*) (**D**) *short gastrulation* (*sog*) (**E**) *single-minded* (*sim*) (**F**) *Kruppel* (*Kr*). Analyzed enhancer regions at these loci are shown as purple (active enhancer region) or red (not active enhancer region) boxes underneath the ATAC profiles. gt enh and KrA enh - KrD enh were tested in *Tribolium*. Other enhancer regions were evaluated in a cross-species context in *Drosophila*. Differential ATAC peaks match well with active enhancer regions of *lab*, *wg*, *D*, and *sim* (A, B, C, E). No differential ATAC peak overlap with the previously described active enhancer region for *sog* (D). Not active KrB enh region is not overlapping with differential ATAC peaks (F), while overlaps are observed between differential ATAC peaks and not active KrA enh, KrC enh, and KrD enh regions (G). ATAC tracks were created with pygenometracks.

Supplementary Figure 8. Simulations with different static enhancer strength. Simulation of dynamic and static enhancer activity and resulting endogenous gene expression. Analyzed was their spatiotemporal behavior. (**A**) dynamic enhancer strength d=3, static enhancer strength c=0; (**B**) d=3, c=0.5; (**C**) d=3; c=1; (**D**) d=3, c=1.5 Left: Intensity plots. Right: Kymographs.

Supplementary Table 1: List of used primers. frw: forward, rev: reverse.

Description	Sequence (5` - 3`)
pBPGUw promoter frw + BsaI into NotI	AAATTTGGTCTCCGGCCGCGATCGAGCGCAGCGGTATAAAA
pBPGUw promoter rev + BsaI into BamHI	AAATTTGGTCTCGGATCCGTTTGGTATGCGTCTTGTGATTCAAAG
pBPGUw promoter-24xMS2-y frw + HindIII	AAATTTAAGCTTGATCGAGCGCAGCGGTATAAAA
pBPGUw promoter-24xMS2-y rev + STOP + SbfI	AAATTTCCTGCAGGTTAACCCACAGAATTTGTAGAGACACTAATACTG
DSCP frw + HindIII	AAATTTAAGCTTGATAAACGGCCGGCAGCGGTATAAAAGGG
DSCP rev + BsaI into BamHI	AAATTTGGTCTCGGATCCGGGCTGCAGATTGTTTAGCTTGTTCAGC
hbA frw + BsaI into XmaI	AAATTTGGTCTCCCCGGGCACCCTATTTACGCAACGGCTATTTTC
hbA rev + BsaI into HindIII	AAATTTGGTCTCAAGCTTTGGTGGAGATGTTATGGTATGGTCG
hbB frw + XmaI	AAATTTCCCGGGCACCCATTGTGACAGCTCGG
hbB rev + HindIII	AAATTTAAGCTTTTCTCTGAGGCATAATCCCACTAATTACC
runA frw + XmaI	AAATTTCCCGGGGGGTAGTTGTCGGTTAGATGCAATATTGTG
runA rev + HindIII	AAATTTAAGCTTCGTTATTCGGAGGTGTCCATTATTGGAAGG
runB frw + XmaI	AAATTTCCCGGGCGCAGCGTTATGAAAAATACGGAACAA
runB rev + HindIII	AAATTTAAGCTTCCGCCTAGCGAGCATTAGTGC
runC frw + BsaI into XmaI	AAATTTGGTCTCCCCGGGGGCTAACATTTGATTCGCACATCGG
runC rev + BsaI into HindIII	AAATTTGGTCTCAAGCTTCCTTGTTCAGCAATCACTCAAATATTGTGC
KrA frw + BsaI into XmaI	AAATTTGGTCTCCCCGGGAATAATTCCGAAACGCAAAGAGATAGACCC
KrA rev + BsaI into HindIII	AAATTTGGTCTCAAGCTTGTGGCATCAAATGGTAGTGACACATCG
KrB frw + BsaI into XmaI	AAATTTGGTCTCCCCGGGGTGGCATCAAGTAGTAGTGAGACATCG
KrB rev + BsaI into HindIII	AAATTTGGTCTCAAGCTTCTAACGGTGTAGGGTTTGCATAGCAAA
KrC frw + BsaI into XmaI	AAATTTGGTCTCCCCGGGTAATCTGAGGAGGCGACGTCTAGC
KrC rev + BsaI into HindIII	AAATTTGGTCTCAAGCTTCGATGTCTCACTACTACTTGATGCCAC
KrD frw + BsaI into XmaI	AAATTTGGTCTCCCCGGGTTCCATAGCCGACTTGATGCACAACC
KrD rev + BsaI into HindIII	AAATTTGGTCTCAAGCTTGCTAGACGTCGCCTCCTCAGATTC

References

1. Spitz F, Furlong EEM. Transcription factors: from enhancer binding to developmental control. Nat Rev Genet. 2012 Sep;13(9):613–626.

2. Shlyueva D, Stampfel G, Stark A. Transcriptional enhancers: from properties to genome-wide predictions. Nat Rev Genet. 2014 Apr;15(4):272–286.

3. Small S, Blair A, Levine M. Regulation of even-skipped stripe 2 in the Drosophila embryo. EMBO J. 1992 Nov;11(11):4047–4057.

4. Clyde DE, Corado MSG, Wu X, Paré A, Papatsenko D, Small S. A self-organizing system of repressor gradients establishes segmental complexity in Drosophila. Nature. 2003 Dec 18;426(6968):849–853.

5. Hoch M, Seifert E, Jäckle H. Gene expression mediated by cis-acting sequences of the Krüppel gene in response to the Drosophila morphogens bicoid and hunchback. EMBO J. 1991 Aug;10(8):2267–2278.

6. Diaz-Cuadros M, Pourquié O, El-Sherif E. Patterning with clocks and genetic cascades: segmentation and regionalization of vertebrate vs. insect body plans. Invited to PLOS Genetics; Under Review. 2021;

7. Clark E, Peel AD, Akam M. Arthropod segmentation. Development. 2019 Sep 25;146(18).

8. Lynch JA, El-Sherif E, Brown SJ. Comparisons of the embryonic development of Drosophila, Nasonia, and Tribolium. Wiley Interdiscip Rev Dev Biol. 2012 Feb;1(1):16–39.

9. Jaeger J. The gap gene network. Cell Mol Life Sci. 2011 Jan;68(2):243–274.

10. Palmeirim I, Henrique D, Ish-Horowicz D, Pourquié O. Avian hairy gene expression identifies a molecular clock linked to vertebrate segmentation and somitogenesis. Cell. 1997 Nov 28;91(5):639–648.

11. Oates AC, Morelli LG, Ares S. Patterning embryos with oscillations: structure, function and dynamics of the vertebrate segmentation clock. Development. 2012 Feb;139(4):625–639.

12. Forlani S, Lawson KA, Deschamps J. Acquisition of Hox codes during gastrulation and axial elongation in the mouse embryo. Development. 2003 Aug 1;130(16):3807–3819.

13. Gaunt SJ, Strachan L. Forward spreading in the establishment of a vertebrate Hox expression boundary: the expression domain separates into anterior and posterior zones, and the spread occurs across implanted glass barriers. Dev Dyn. 1994 Mar;199(3):229–240.

14. Dessaud E, Yang LL, Hill K, Cox B, Ulloa F, Ribeiro A, et al. Interpretation of the sonic hedgehog morphogen gradient by a temporal adaptation mechanism. Nature. 2007 Nov 29;450(7170):717–720.

15. Balaskas N, Ribeiro A, Panovska J, Dessaud E, Sasai N, Page KM, et al. Gene regulatory logic for reading the Sonic Hedgehog signaling gradient in the vertebrate neural tube. Cell. 2012 Jan 20;148(1-2):273–284.

16. Harfe BD, Scherz PJ, Nissim S, Tian H, McMahon AP, Tabin CJ. Evidence for an expansion-based temporal Shh gradient in specifying vertebrate digit identities. Cell. 2004 Aug 20;118(4):517–528.

17. Saiz-Lopez P, Chinnaiya K, Campa VM, Delgado I, Ros MA, Towers M. An intrinsic timer specifies distal structures of the vertebrate limb. Nat Commun. 2015 Sep 18;6:8108.

18. Roensch K, Tazaki A, Chara O, Tanaka EM. Progressive specification rather than intercalation of segments during limb regeneration. Science. 2013 Dec 13;342(6164):1375–1379.

19. Towers M, Tickle C. Growing models of vertebrate limb development. Development. 2009 Jan;136(2):179–190.

20. El-Sherif E, Averof M, Brown SJ. A segmentation clock operating in blastoderm and germband stages of Tribolium development. Development. 2012 Dec 1;139(23):4341–4346.

21. Sarrazin AF, Peel AD, Averof M. A segmentation clock with two-segment periodicity in insects. Science. 2012 Apr 20;336(6079):338–341.

22. El-Sherif E, Zhu X, Fu J, Brown SJ. Caudal regulates the spatiotemporal dynamics of pair-rule waves in Tribolium. PLoS Genet. 2014 Oct 16;10(10):e1004677.

23. Zhu X, Rudolf H, Healey L, François P, Brown SJ, Klingler M, et al. Speed regulation of genetic cascades allows for evolvability in the body plan specification of insects. Proc Natl Acad Sci USA. 2017 Sep 25;114(41).

24. Boos A, Distler J, Rudolf H, Klingler M, El-Sherif E. A re-inducible gap gene cascade patterns the anterior-posterior axis of insects in a threshold-free fashion. Elife. 2018 Dec 20;7.

25. Jaeger J, Surkova S, Blagov M, Janssens H, Kosman D, Kozlov KN, et al. Dynamic control of positional information in the early Drosophila embryo. Nature. 2004 Jul 15;430(6997):368–371.

26. El-Sherif E, Levine M. Shadow enhancers mediate dynamic shifts of gap gene expression in the drosophila embryo. Curr Biol. 2016 May 9;26(9):1164–1169.

27. Lim B, Fukaya T, Heist T, Levine M. Temporal dynamics of pair-rule stripes in living Drosophila embryos. Proc Natl Acad Sci USA. 2018 Aug 14;115(33):8376–8381.

28. Berrocal A, Lammers NC, Garcia HG, Eisen MB. Kinetic sculpting of the seven stripes of the Drosophila even-skipped gene. Elife. 2020 Dec 10;9.

29. Keränen SVE, Fowlkes CC, Luengo Hendriks CL, Sudar D, Knowles DW, Malik J, et al. Three-dimensional morphology and gene expression in the Drosophila blastoderm at cellular resolution II: dynamics. Genome Biol. 2006;7(12):R124.

30. Rudolf H, Zellner C, El-Sherif E. Speeding up anterior-posterior patterning of insects by differential initialization of the gap gene cascade. Dev Biol. 2020 Apr 1;460(1):20–31.

31. Verd B, Clark E, Wotton KR, Janssens H, Jiménez-Guri E, Crombach A, et al. A damped oscillator imposes temporal order on posterior gap gene expression in Drosophila. PLoS Biol. 2018 Feb 16;16(2):e2003174.

32. Clark E, Peel AD. Evidence for the temporal regulation of insect segmentation by a conserved sequence of transcription factors. Development. 2018 May 3;

33. Clark E. Dynamic patterning by the Drosophila pair-rule network reconciles long-germ and short-germ segmentation. PLoS Biol. 2017 Sep 27;15(9):e2002439.

34. Kuhlmann L, El-Sherif E. Speed regulation and gradual enhancer switching models as flexible and evolvable patterning mechanisms. BioRxiv. 2018 Feb 7;

35. Hoermann A, Cicin-Sain D, Jaeger J. A quantitative validated model reveals two phases of transcriptional regulation for the gap gene giant in Drosophila. Dev Biol. 2016 Mar 15;411(2):325–338.

36. Bucher G, Scholten J, Klingler M. Parental rnai in tribolium (coleoptera). Curr Biol. 2002 Feb 5;12(3):R85–6.

37. Miller SC, Miyata K, Brown SJ, Tomoyasu Y. Dissecting systemic RNA interference in the red flour beetle Tribolium castaneum: parameters affecting the efficiency of RNAi. PLoS One. 2012 Oct 25;7(10):e47431.

38. Tomoyasu Y, Miller SC, Tomita S, Schoppmeier M, Grossmann D, Bucher G. Exploring systemic RNA interference in insects: a genome-wide survey for RNAi genes in Tribolium. Genome Biol. 2008 Jan 17;9(1):R10.

39. Dönitz J, Schmitt-Engel C, Grossmann D, Gerischer L, Tech M, Schoppmeier M, et al. iBeetle-Base: a database for RNAi phenotypes in the red flour beetle Tribolium castaneum. Nucleic Acids Res. 2015 Jan;43(Database issue):D720–5.

40. Choe CP, Brown SJ. Genetic regulation of engrailed and wingless in Tribolium segmentation and the evolution of pair-rule segmentation. Dev Biol. 2009 Jan 15;325(2):482–491.

41. Bolognesi R, Beermann A, Farzana L, Wittkopp N, Lutz R, Balavoine G, et al. Tribolium Wnts: evidence for a larger repertoire in insects with overlapping expression patterns that suggest multiple redundant functions in embryogenesis. Dev Genes Evol. 2008 Apr 8;218(3-4):193–202.

42. Choe CP, Miller SC, Brown SJ. A pair-rule gene circuit defines segments sequentially in the short-germ insect Tribolium castaneum. Proc Natl Acad Sci USA. 2006 Apr 25;103(17):6560–6564.

43. Kotkamp K, Klingler M, Schoppmeier M. Apparent role of Tribolium orthodenticle in anteroposterior blastoderm patterning largely reflects novel functions in dorsoventral axis formation and cell survival. Development. 2010 Jun;137(11):1853–1862.

44. Schoppmeier M, Fischer S, Schmitt-Engel C, Löhr U, Klingler M. An ancient anterior patterning system promotes caudal repression and head formation in ecdysozoa. Curr Biol. 2009 Nov 17;19(21):1811–1815.

45. Cerny AC, Bucher G, Schröder R, Klingler M. Breakdown of abdominal patterning in the Tribolium Kruppel mutant jaws. Development. 2005 Dec;132(24):5353–5363.

46. Bucher G, Klingler M. Divergent segmentation mechanism in the short germ insect Tribolium revealed by giant expression and function. Development. 2004 Apr;131(8):1729–1740.

47. Schmitt-Engel C, Cerny AC, Schoppmeier M. A dual role for nanos and pumilio in anterior and posterior blastodermal patterning of the short-germ beetle Tribolium castaneum. Dev Biol. 2012 Apr 15;364(2):224–235.

48. Marques-Souza H, Aranda M, Tautz D. Delimiting the conserved features of hunchback function for the trunk organization of insects. Development. 2008 Mar;135(5):881–888.

49. Savard J, Marques-Souza H, Aranda M, Tautz D. A segmentation gene in tribolium produces a polycistronic mRNA that codes for multiple conserved peptides. Cell. 2006 Aug 11;126(3):559–569.

50. Marques-Souza H. Evolution of the gene regulatory network controlling trunk segmentation in insects [Doctoral dissertation]. University of Cologne; 2007.

51. Klingler M, Bucher G. The red flour beetle T. castaneum: elaborate genetic toolkit and unbiased large scale RNAi screening to study insect biology and evolution. Evodevo. 2022 Dec;13(1):14.

52. Pavlopoulos A, Berghammer AJ, Averof M, Klingler M. Efficient transformation of the beetle Tribolium castaneum using the Minos transposable element: quantitative and qualitative analysis of genomic integration events. Genetics. 2004 Jun;167(2):737–746.

53. Strobl F, Anderl A, Stelzer EH. A universal vector concept for a direct genotyping of transgenic organisms and a systematic creation of homozygous lines. Elife. 2018 Mar 15;7.

54. Trauner J, Schinko J, Lorenzen MD, Shippy TD, Wimmer EA, Beeman RW, et al. Large-scale insertional mutagenesis of a coleopteran stored grain pest, the red flour beetle Tribolium castaneum, identifies embryonic lethal mutations and enhancer traps. BMC Biol. 2009 Nov 5;7:73.

55. Gilles AF, Schinko JB, Averof M. Efficient CRISPR-mediated gene targeting and transgene replacement in the beetle Tribolium castaneum. Development. 2015 Aug 15;142(16):2832–2839.

56. Gilles AF, Schinko JB, Schacht MI, Enjolras C, Averof M. Clonal analysis by tunable CRISPR-mediated excision. Development. 2019 Jan 4;146(1).

57. Strobl F, Stelzer EH. Long-term fluorescence live imaging of Tribolium castaneum embryos: principles, resources, scientific challenges and the comparative approach. Curr Opin Insect Sci. 2016 Aug 28;18:17–26.

58. Strobl F, Stelzer EHK. Non-invasive long-term fluorescence live imaging of Tribolium castaneum embryos. Development. 2014 Jun;141(11):2331–2338.

59. Strobl F, Schmitz A, Stelzer EHK. Live imaging of Tribolium castaneum embryonic development using light-sheet-based fluorescence microscopy. Nat Protoc. 2015 Oct;10(10):1486–1507.

60. Macaya CC, Saavedra PE, Cepeda RE, Nuñez VA, Sarrazin AF. A Tribolium castaneum whole-embryo culture protocol for studying the molecular mechanisms and morphogenetic movements involved in insect development. Dev Genes Evol. 2016 Jan 6;226(1):53–61.

61. Buenrostro JD, Giresi PG, Zaba LC, Chang HY, Greenleaf WJ. Transposition of native chromatin for fast and sensitive epigenomic profiling of open chromatin, DNA-binding proteins and nucleosome position. Nat Methods. 2013 Dec;10(12):1213–1218.

62. Thurman RE, Rynes E, Humbert R, Vierstra J, Maurano MT, Haugen E, et al. The accessible chromatin landscape of the human genome. Nature. 2012 Sep 6;489(7414):75–82.

63. Kok K, Arnosti DN. Dynamic reprogramming of chromatin: paradigmatic palimpsests and HES factors. Front Genet. 2015 Feb 10;6:29.

64. Xi H, Shulha HP, Lin JM, Vales TR, Fu Y, Bodine DM, et al. Identification and characterization of cell type-specific and ubiquitous chromatin regulatory structures in the human genome. PLoS Genet. 2007 Aug;3(8):e136.

65. Li LM, Arnosti DN. Long- and short-range transcriptional repressors induce distinct chromatin states on repressed genes. Curr Biol. 2011 Mar 8;21(5):406–412.

66. Reddington JP, Garfield DA, Sigalova OM, Karabacak Calviello A, Marco-Ferreres R, Girardot C, et al. Lineage-Resolved Enhancer and Promoter Usage during a Time Course of Embryogenesis. Dev Cell. 2020 Dec 7;55(5):648–664.e9.

67. Bozek M, Cortini R, Storti AE, Unnerstall U, Gaul U, Gompel N. ATAC-seq reveals regional differences in enhancer accessibility during the establishment of spatial coordinates in the Drosophila blastoderm. Genome Res. 2019 May;29(5):771–783.

68. McKay DJ, Lieb JD. A common set of DNA regulatory elements shapes Drosophila appendages. Dev Cell. 2013 Nov 11;27(3):306–318.

69. Li X, Zhao X, Fang Y, Jiang X, Duong T, Fan C, et al. Generation of destabilized green fluorescent protein as a transcription reporter. J Biol Chem. 1998 Dec 25;273(52):34970–34975.

70. He L, Binari R, Huang J, Falo-Sanjuan J, Perrimon N. In vivo study of gene expression with an enhanced dual-color fluorescent transcriptional timer. Elife. 2019 May 29;8.

71. Pichon X, Lagha M, Mueller F, Bertrand E. A growing toolbox to image gene expression in single cells: sensitive approaches for demanding challenges. Mol Cell. 2018 Aug 2;71(3):468–480.

72. Johansson HE, Liljas L, Uhlenbeck OC. RNA recognition by the MS2 phage coat protein. Seminars in virology. 1997;8(3):176–185.

73. Garcia HG, Tikhonov M, Lin A, Gregor T. Quantitative imaging of transcription in living Drosophila embryos links polymerase activity to patterning. Curr Biol. 2013 Nov 4;23(21):2140–2145.

74. Lucas T, Ferraro T, Roelens B, De Las Heras Chanes J, Walczak AM, Coppey M, et al. Live imaging of bicoid-dependent transcription in Drosophila embryos. Curr Biol. 2013 Nov 4;23(21):2135–2139.

75. Bothma JP, Garcia HG, Esposito E, Schlissel G, Gregor T, Levine M. Dynamic regulation of eve stripe 2 expression reveals transcriptional bursts in living Drosophila embryos. Proc Natl Acad Sci USA. 2014 Jul 22;111(29):10598–10603.

76. Dufourt J, Bellec M, Trullo A, Dejean M, De Rossi S, Favard C, et al. Imaging translation dynamics in live embryos reveals spatial heterogeneities. Science. 2021 May 21;372(6544):840–844.

77. Lai Y-T, Deem KD, Borràs-Castells F, Sambrani N, Rudolf H, Suryamohan K, et al. Enhancer identification and activity evaluation in the red flour beetle, Tribolium castaneum. Development. 2018 Apr 5;145(7).

78. Simon JM, Giresi PG, Davis IJ, Lieb JD. Using formaldehyde-assisted isolation of regulatory elements (FAIRE) to isolate active regulatory DNA. Nat Protoc. 2012 Jan 19;7(2):256–267.

79. Blythe SA, Wieschaus EF. Establishment and maintenance of heritable chromatin structure during early Drosophila embryogenesis. Elife. 2016 Nov 23;5.

80. Cande J, Goltsev Y, Levine MS. Conservation of enhancer location in divergent insects. Proc Natl Acad Sci USA. 2009 Aug 25;106(34):14414–14419.

81. Kazemian M, Suryamohan K, Chen J-Y, Zhang Y, Samee MAH, Halfon MS, et al. Evidence for deep regulatory similarities in early developmental programs across highly diverged insects. Genome Biol Evol. 2014 Sep;6(9):2301–2320.

82. Bailles A, Gehrels EW, Lecuit T. Mechanochemical principles of spatial and temporal patterns in cells and tissues. Annu Rev Cell Dev Biol. 2022 May 13;

83. Di Talia S, Vergassola M. Waves in embryonic development. Annu Rev Biophys. 2022 May 9;51:327–353.

84. Pfeiffer BD, Jenett A, Hammonds AS, Ngo T-TB, Misra S, Murphy C, et al. Tools for neuroanatomy and neurogenetics in Drosophila. Proc Natl Acad Sci USA. 2008 Jul 15;105(28):9715–9720.

85. Tribolium Genome Sequencing Consortium, Richards S, Gibbs RA, Weinstock GM, Brown SJ, Denell R, et al. The genome of the model beetle and pest Tribolium castaneum. Nature. 2008 Apr 24;452(7190):949–955.

86. Siebert KS, Lorenzen MD, Brown SJ, Park Y, Beeman RW. Tubulin superfamily genes in Tribolium castaneum and the use of a Tubulin promoter to drive transgene expression. Insect Biochem Mol Biol. 2008 Aug;38(8):749–755.

87. Chook YM, Blobel G. Karyopherins and nuclear import. Curr Opin Struct Biol. 2001 Dec;11(6):703–715.

88. Field J, Nikawa J, Broek D, MacDonald B, Rodgers L, Wilson IA, et al. Purification of a RAS-responsive adenylyl cyclase complex from Saccharomyces cerevisiae by use of an epitope addition method. Mol Cell Biol. 1988 May;8(5):2159–2165.

89. Bertrand E, Chartrand P, Schaefer M, Shenoy SM, Singer RH, Long RM. Localization of ASH1 mRNA particles in living yeast. Mol Cell. 1998 Oct;2(4):437–445.

90. Shaner NC, Steinbach PA, Tsien RY. A guide to choosing fluorescent proteins. Nat Methods. 2005 Dec;2(12):905–909.

91. Li X, Harrell RA, Handler AM, Beam T, Hennessy K, Fraser MJ. piggyBac internal sequences are necessary for efficient transformation of target genomes. Insect Mol Biol. 2005 Jan;14(1):17–30.

92. Shaner NC, Lin MZ, McKeown MR, Steinbach PA, Hazelwood KL, Davidson MW, et al. Improving the photostability of bright monomeric orange and red fluorescent proteins. Nat Methods. 2008 Jun;5(6):545–551.

93. Shaner NC, Campbell RE, Steinbach PA, Giepmans BNG, Palmer AE, Tsien RY. Improved monomeric red, orange and yellow fluorescent proteins derived from Discosoma sp. red fluorescent protein. Nat Biotechnol. 2004 Dec;22(12):1567–1572.

94. Berghammer AJ, Klingler M, Wimmer EA. A universal marker for transgenic insects. Nature. 1999 Nov 25;402(6760):370–371.

95. Handler AM, Harrell RA. Germline transformation of Drosophila melanogaster with the piggyBac transposon vector. Insect Mol Biol. 1999 Nov;8(4):449–457.

96. Lorenzen MD, Berghammer AJ, Brown SJ, Denell RE, Klingler M, Beeman RW. piggyBac-mediated germline transformation in the beetle Tribolium castaneum. Insect Mol Biol. 2003 Oct;12(5):433–440.

97. Berghammer AJ, Weber M, Trauner J, Klingler M. Red flour beetle (Tribolium) germline transformation and insertional mutagenesis. Cold Spring Harb Protoc. 2009 Aug;2009(8):pdb.prot5259.

98. Lorenzen MD, Brown SJ, Denell RE, Beeman RW. Cloning and characterization of the Tribolium castaneum eye-color genes encoding tryptophan oxygenase and kynurenine 3-monooxygenase. Genetics. 2002 Jan;160(1):225–234.

99. Handler AM. Use of the piggyBac transposon for germ-line transformation of insects. Insect Biochem Mol Biol. 2002 Oct;32(10):1211–1220.

100. Choi HMT, Schwarzkopf M, Fornace ME, Acharya A, Artavanis G, Stegmaier J, et al. Third-generation in situ hybridization chain reaction: multiplexed, quantitative, sensitive, versatile, robust. Development. 2018 Jun 26;145(12).

101. Schindelin J, Arganda-Carreras I, Frise E, Kaynig V, Longair M, Pietzsch T, et al. Fiji: an open-source platform for biological-image analysis. Nat Methods. 2012 Jun 28;9(7):676–682.

102. Buenrostro JD, Wu B, Chang HY, Greenleaf WJ. ATAC-seq: a method for assaying chromatin accessibility genome-wide. Curr Protoc Mol Biol. 2015 Jan 5;109:21.29.1–21.29.9.

103. Danecek P, Bonfield JK, Liddle J, Marshall J, Ohan V, Pollard MO, et al. Twelve years of SAMtools and BCFtools. Gigascience. 2021 Feb 16;10(2).

104. Amemiya HM, Kundaje A, Boyle AP. The ENCODE blacklist: identification of problematic regions of the genome. Sci Rep. 2019 Jun 27;9(1):9354.

105. Pongor LS, Gross JM, Vera Alvarez R, Murai J, Jang S-M, Zhang H, et al. BAMscale: quantification of next-generation sequencing peaks and generation of scaled coverage tracks. Epigenetics Chromatin. 2020 Apr 22;13(1):21.

106. Zhang Y, Liu T, Meyer CA, Eeckhoute J, Johnson DS, Bernstein BE, et al. Model-based analysis of ChIP-Seq (MACS). Genome Biol. 2008 Sep 17;9(9):R137.

107. Heinz S, Benner C, Spann N, Bertolino E, Lin YC, Laslo P, et al. Simple combinations of lineage-determining transcription factors prime cis-regulatory elements required for macrophage and B cell identities. Mol Cell. 2010 May 28;38(4):576–589.

108. Robinson MD, McCarthy DJ, Smyth GK. edgeR: a Bioconductor package for differential expression analysis of digital gene expression data. Bioinformatics. 2010 Jan 1;26(1):139–140.

109. Love MI, Huber W, Anders S. Moderated estimation of fold change and' ' dispersion for RNA-seq data with DESeq2. Genome Biol. 2014;15(12):550.

110. Robinson MD, Oshlack A. A scaling normalization method for differential expression analysis of RNA-seq data. Genome Biol. 2010 Mar 2;11(3):R25.

111. Castro-Mondragon JA, Riudavets-Puig R, Rauluseviciute I, Lemma RB, Turchi L, Blanc-Mathieu R, et al. JASPAR 2022: the 9th release of the open-access database of transcription factor binding profiles. Nucleic Acids Res. 2022 Jan 7;50(D1):D165–D173.

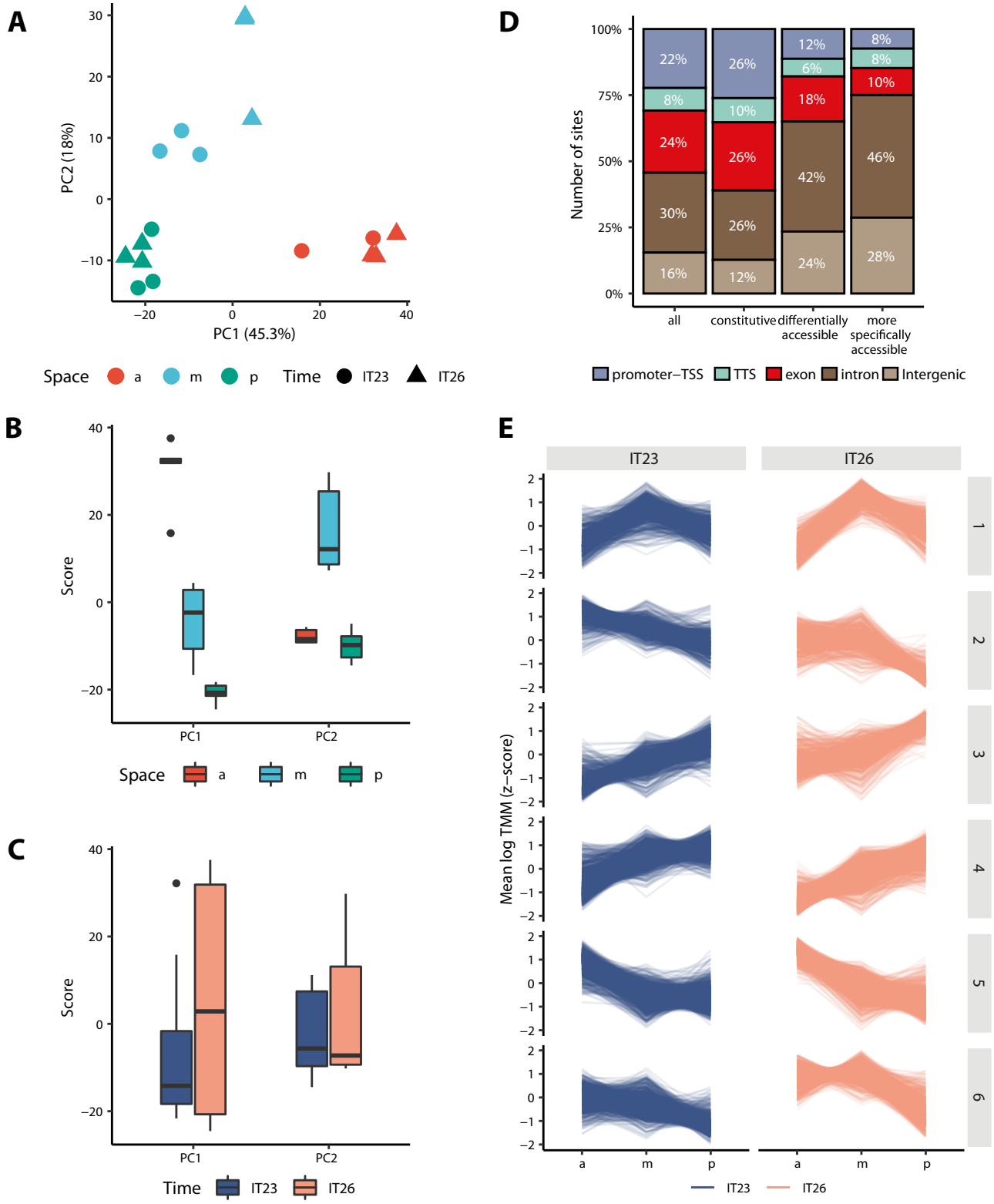

Figure 1: Chromatin accessibility changes during AP axis patterning in the *Tribolium* embryo.

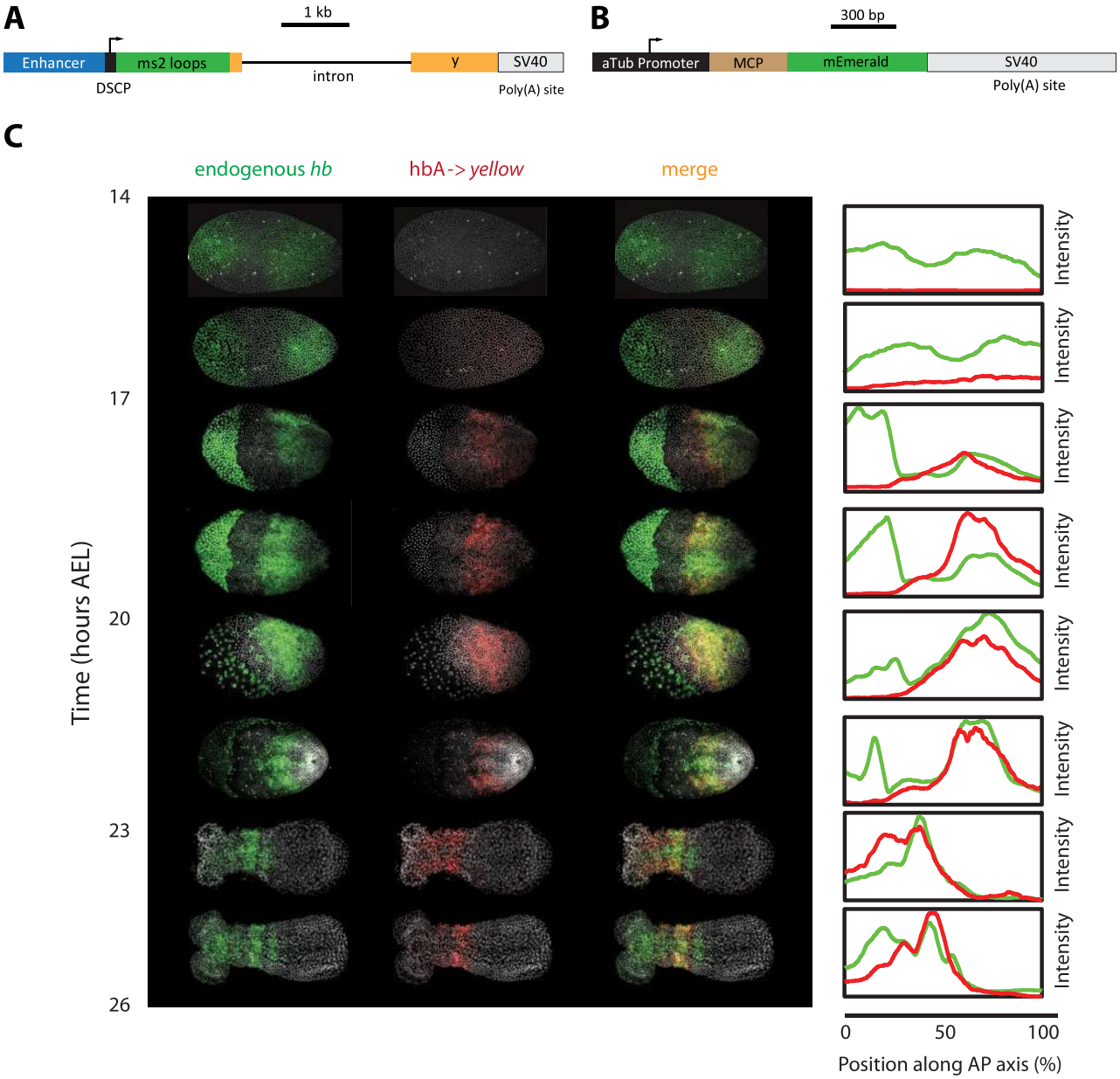

Figure 2: Analysis of hbA enhancer reporter construct.

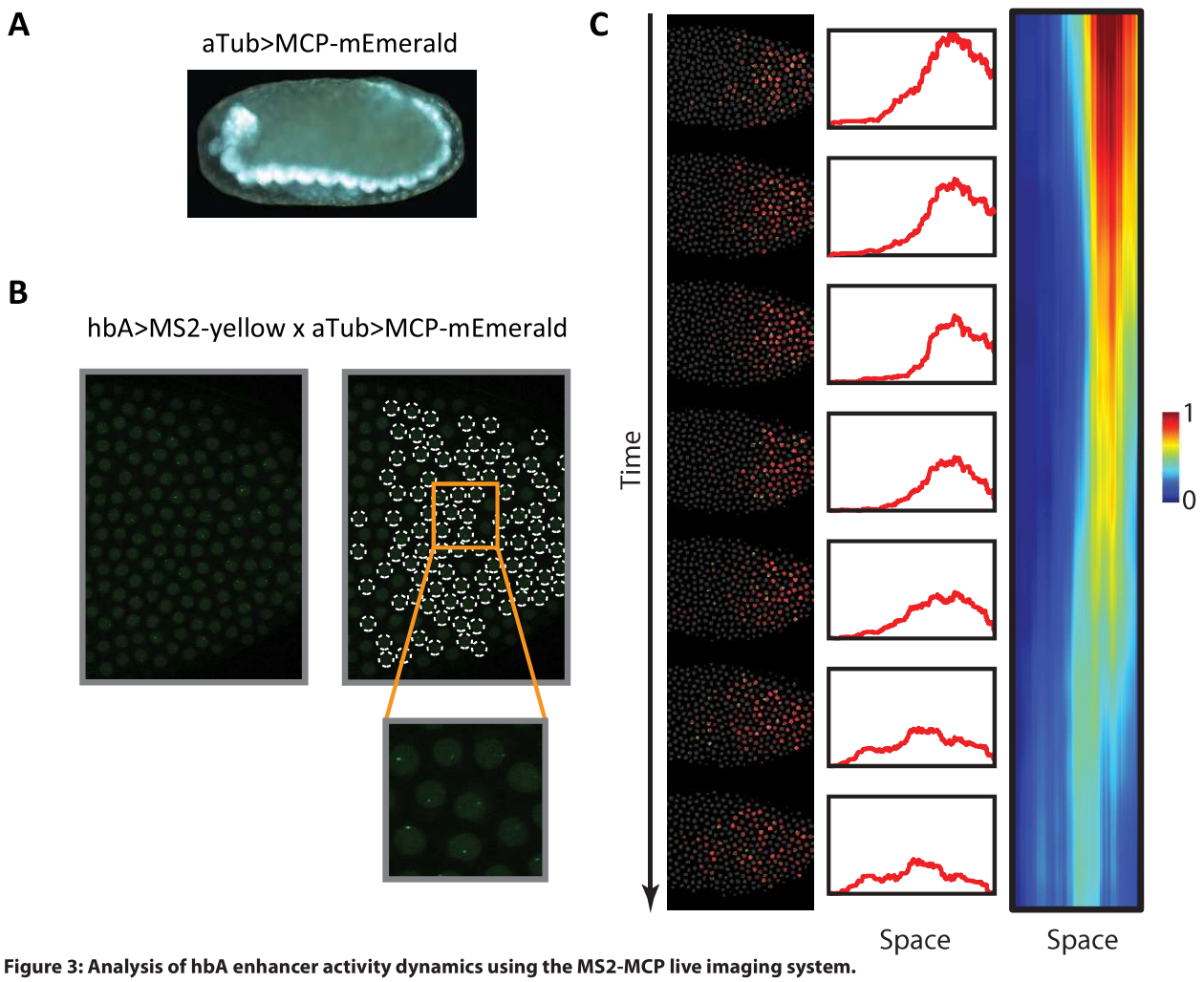

Figure 3: Analysis of hbA enhancer activity dynamics using the MS2-MCP live imaging system.

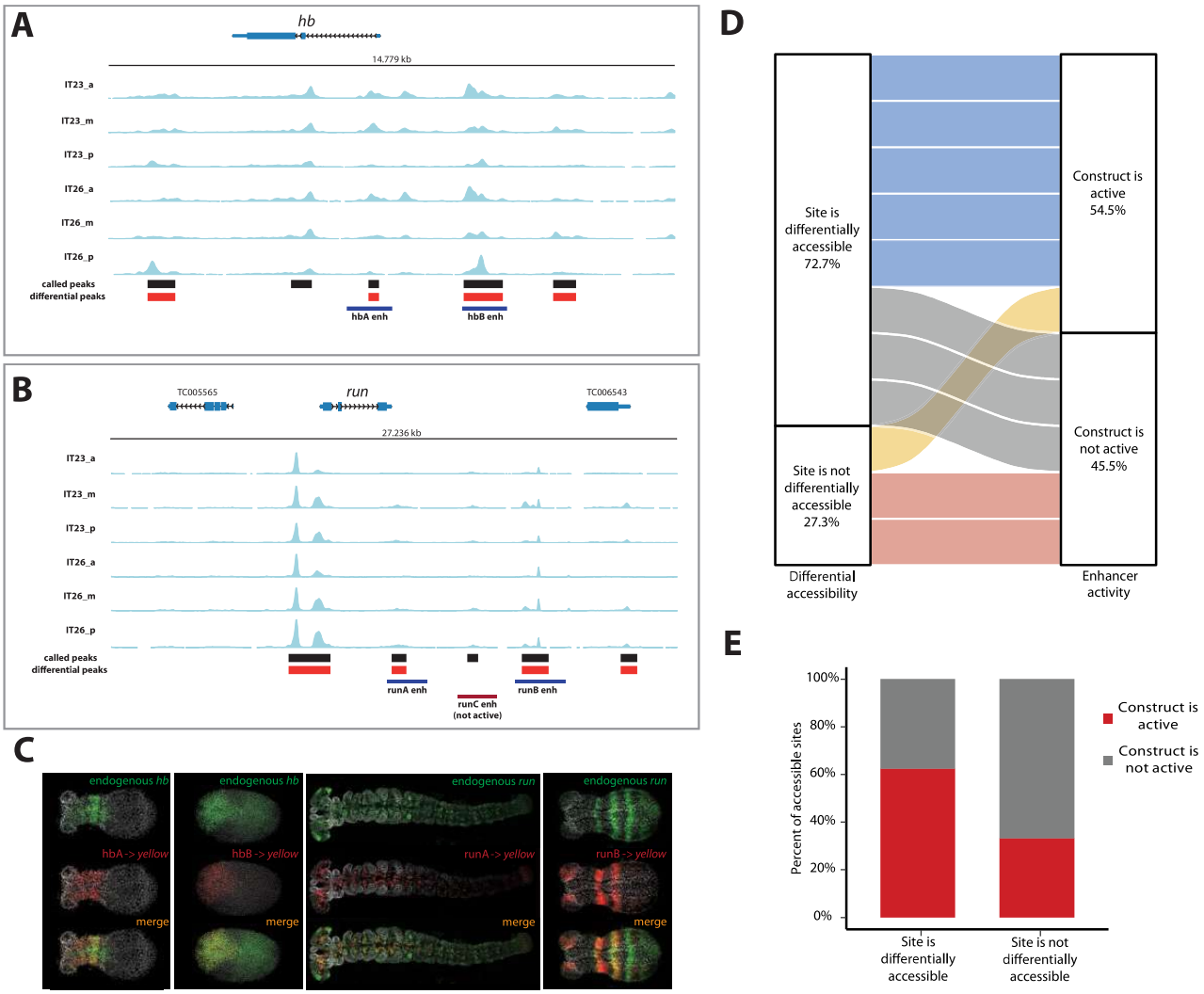

Figure 4: Differential peak analysis of examined enhancer constructs.

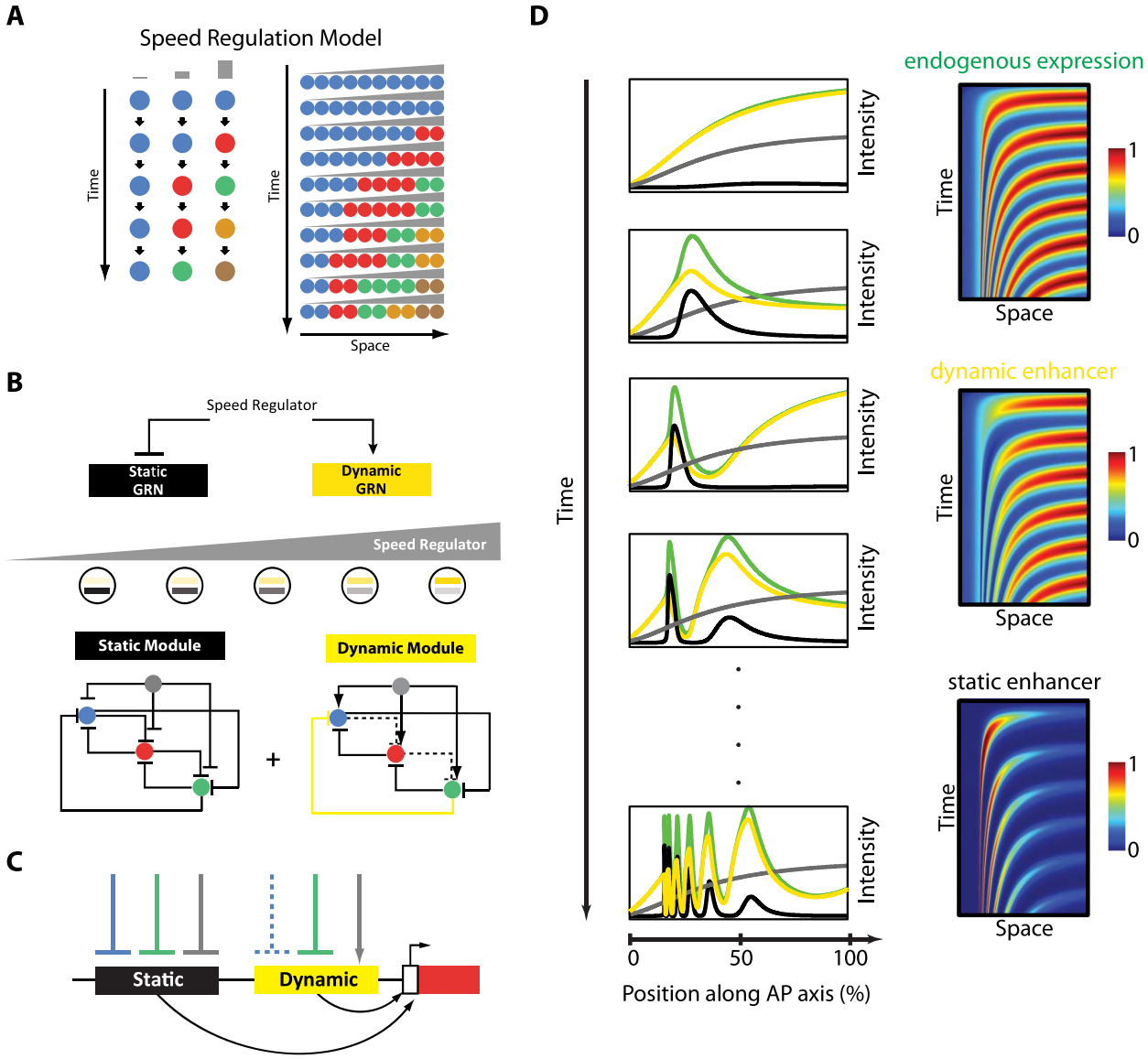

Figure 5: Simulation of spatiotemporal dynamics of dynamic and static enhancer activity.

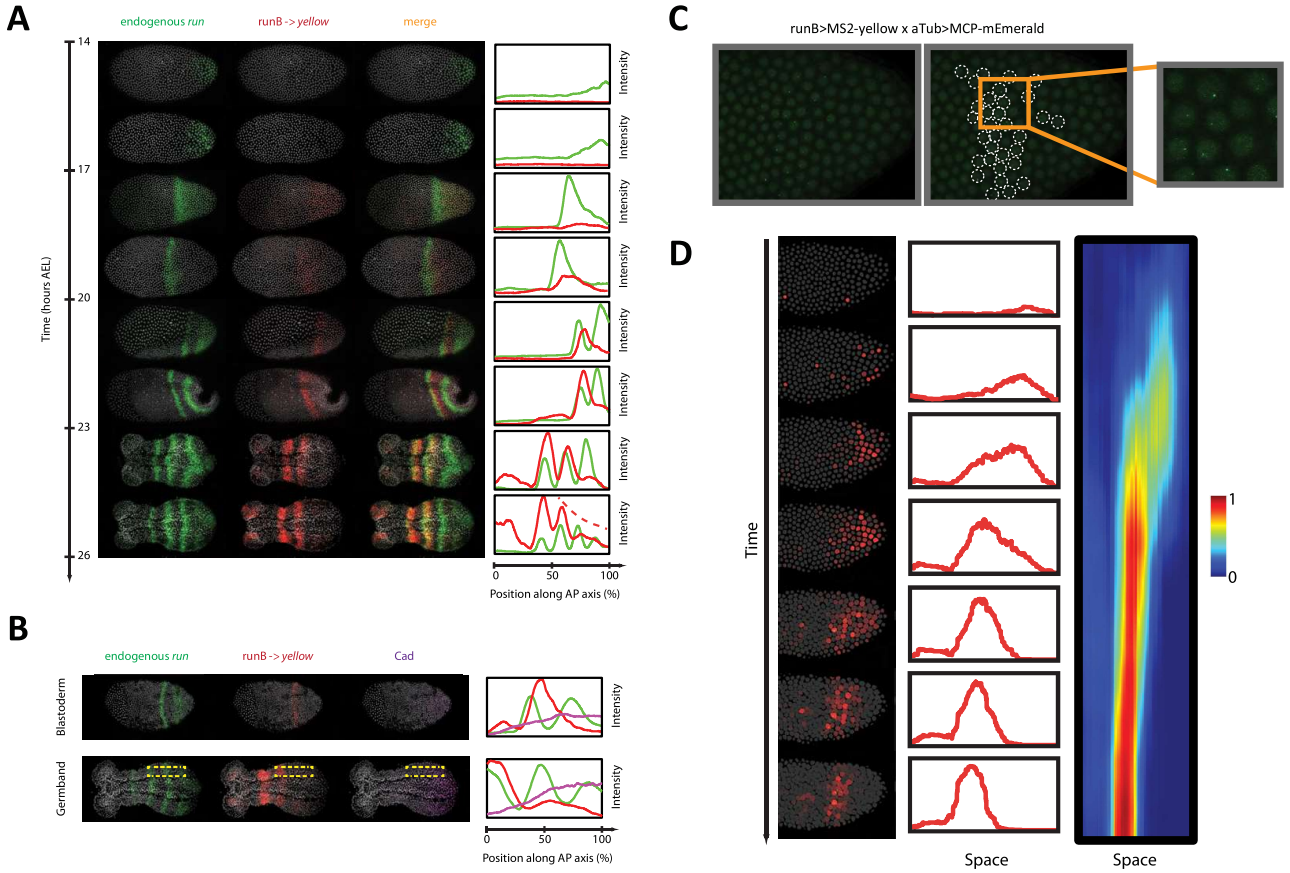

Figure 6: Analysis of runB enhancer activity dynamics using *in situ* staining and the MS2-MCP live imaging system.